

# Thermal properties, phase transitions, vibrational and reorientational dynamics of $[\text{Mn}(\text{NH}_3)_6](\text{NO}_3)_2$

Edward Mikuli · Marta Liszka-Skoczylas ·  
Joanna Hetmańczyk · Janusz Szklarzewicz

Received: 22 January 2010 / Accepted: 23 March 2010 / Published online: 10 April 2010  
© Akadémiai Kiadó, Budapest, Hungary 2010

**Abstract**  $[\text{Mn}(\text{NH}_3)_6](\text{NO}_3)_2$  crystallizes in the cubic, fluorite (C1) type crystal lattice structure ( $Fm \bar{3}m$ ) with  $a = 11.0056 \text{ \AA}$  and  $Z = 4$ . Two phase transitions of the first-order type were detected. The first registered on DSC curves as a large anomaly at  $T_{C1}^h = 207.8 \text{ K}$  and  $T_{C1}^c = 207.2 \text{ K}$ , and the second registered as a smaller anomaly at  $T_{C2}^h = 184.4 \text{ K}$  and  $T_{C2}^c = 160.8 \text{ K}$  (where the upper indexes h and c denote heating and cooling of the sample, respectively). The temperature dependence of the full width at half maximum of the band associated with the  $\delta_s(\text{HNH})\text{F}_{1u}$  mode suggests that the  $\text{NH}_3$  ligands in the high temperature and intermediate phase reorientate quickly with correlation times in the order of several picoseconds and with activation energy of  $9.9 \text{ kJ mol}^{-1}$ . In the phase transition at  $T_{C2}^c$  probably only a some of the  $\text{NH}_3$  ligands stop their reorientation, while the remainders continue to reorientate quickly with activation energy of  $7.7 \text{ kJ mol}^{-1}$ . Thermal decomposition of the investigated compound starts at  $305 \text{ K}$  and continues up to  $525 \text{ K}$  in four main stages (I–IV). In stage I,  $2/6$  of all  $\text{NH}_3$  ligands were seceded. Stages II and III are connected with an abruptness of the next  $2/6$  and  $1/6$  of total  $\text{NH}_3$ , respectively, and  $[\text{Mn}(\text{NH}_3)_6](\text{NO}_3)_2$  is formed. The last molecule of  $\text{NH}_3$  per formula unit is freed at stage IV together with the simultaneous thermal decomposition of the resulting  $\text{Mn}(\text{NO}_3)_2$  leading to the formation of gaseous products ( $\text{O}_2$ ,  $\text{H}_2\text{O}$ ,  $\text{N}_2$  and nitrogen oxides) and solid  $\text{MnO}_2$ .

**Keywords** Hexaamminemanganese(II) nitrate(V) · Phase transitions · Ammonia reorientational dynamics · Thermal analysis · DSC · FT-IR · FT-RS · XRPD · TG-DTG-DTA-QMS

## Introduction

The ionic coordination compounds with formula  $[\text{M}(\text{NH}_3)_6](\text{NO}_3)_2$ , where  $\text{M} = \text{Mg, Ni}$ , have a crystal lattice of cubic symmetry ( $fcc$ —a face centred cubic, space group:  $Fm \bar{3}m$  according to Wyckoff [1, 2], fluorite (C1) type, Pearson symbol: cF12, international space group number: 225) at room temperature [1–6], which is possible because both the  $\text{NH}_3$  ligands and the complex anions perform fast reorientational motions with correlation times in the order of picoseconds. On cooling, several phase transitions take place in these compounds [7–11]. For example,  $[\text{Ni}(\text{NH}_3)_6](\text{NO}_3)_2$  displayed four low temperature phases [8–10]. The phase transition at  $T_{C1}$ , associated with the largest change of entropy, was connected with a change in the crystal structure (to the simple cubic phase with space group  $Pa3$ ) [6] and simultaneously it was connected with a drastic change in the speed of the reorientational motions of the  $\text{NO}_3^-$  anions [12, 13]. However, the reorientation of at least some of the  $\text{NH}_3$  ligands [14, 15] still remains fast even below the temperature of liquid nitrogen [14–19]. On further cooling, the phase transition to phase III at  $T_{C2}$  takes place leading to orthorhombic deformation of the crystal lattice. On further cooling, a phase transition at  $T_{C3}$  to phase IV takes place, which leads to a monoclinic lattice deformation [6].

Both  $[\text{Ni}(\text{NH}_3)_6](\text{NO}_3)_2$  and  $[\text{Mg}(\text{NH}_3)_6](\text{NO}_3)_2$  are distinct from many other hexaamminemetal(II) ionic coordination compounds particularly because of the

E. Mikuli (✉) · M. Liszka-Skoczylas · J. Hetmańczyk ·  
J. Szklarzewicz  
Faculty of Chemistry, The Jagiellonian University, Ingardena 3,  
30-060 Kraków, Poland  
e-mail: mikuli@chemia.uj.edu.pl

existence of very large ( $\sim 100$  and  $\sim 40$  K, respectively) thermal hysteresis of the phase transition at  $T_{C2}$  [14–19]. However, for  $[\text{Cd}(\text{NH}_3)_6](\text{NO}_3)_2$  and for  $[\text{Co}(\text{NH}_3)_6](\text{NO}_3)_2$  only one phase transition has been found so far [20, 21].

$[\text{Mn}(\text{NH}_3)_6](\text{NO}_3)_2$  had not previously been investigated from the point of view mentioned above, and so determining its polymorphism was one of the aims of this study. We would also like to compare the results with those obtained earlier for  $[\text{M}(\text{NH}_3)_6](\text{NO}_3)_2$  compounds with  $\text{M} = \text{Ni}^{2+}$ ,  $\text{Mg}^{2+}$ ,  $\text{Cd}^{2+}$  and  $\text{Co}^{2+}$ . In addition, we wanted to establish the progress of the thermal decomposition of hexaamminemanganese(II) nitrate(V) using thermal analysis methods (TG, DTG, QMS, SDTA).

## Experimental procedures

The initial substance used in the synthesis of the title compound was  $[\text{Mn}(\text{H}_2\text{O})_6](\text{NO}_3)_2$ , which was in turn obtained by a reaction of the corresponding carbonate with diluted  $\text{HNO}_3$ . The crystals obtained were re-crystallized three times from double distilled water in a quartz vessel and then dried in a desiccator over  $\text{BaO}$ . The resulting 30 g of  $[\text{Mn}(\text{H}_2\text{O})_6](\text{NO}_3)_2$  was dissolved in 60 mL of acetone. This solution was deoxygenated by the bubbling of argon and, after 20 min, dry gaseous ammonia was also flowed through the solution. The solution became hot, and the precipitation of very light brown (almost white) polycrystalline sediment was observed. The ammonia was purged for as long as it took for the initially warm solutions to cool to room temperature (about 25 min). Flowed ammonia cooled this mixture to room temperature, which was then heated, all the while under a stream of ammonia, to ca. 325 K, over the course of 10 min. Then bubbling of argon was stopped and the mixture was cooled and filtered under a stream of dry ammonia. The solid product (in the form of a light brown polycrystalline powder) was washed three times with acetone saturated with ammonia and twice with diethyl ether. Then it was dried under a stream of dry ammonia over the course of several minutes and transferred to a tightly sealed vessel containing dry ammonia. Before each measurement, the composition of the  $[\text{Mn}(\text{NH}_3)_6](\text{NO}_3)_2$  sample was checked according to its manganese and ammonia content using titration by means of EDTA and HCl, respectively. The average content of  $\text{Mn}^{2+}$  and  $\text{NH}_3$  was 19.09 and 35.95%, theoretical values are 19.54 and 36.34%, respectively. All steps of the analysis were undertaken in an argon atmosphere (Schlenk apparatus) to avoid the oxidation to brown products (probably  $\text{MnO}_2$ ) with simultaneous  $\text{NH}_3$  release.

In order to further confirm the identity of the title compound, thermal analysis was performed using

thermogravimetry with simultaneous differential thermal analysis (TGA/DTG/SDTA) by means of a Mettler Toledo TGA/SDTA 851e apparatus. Evolved gaseous products from the decomposition of the compound were identified on-line using a (QMS) Balzer GSD 300T quadruple mass spectrometer (more details of this experiment are presented in [22]). A sample of mass 8.9733 mg was placed in an open 150  $\mu\text{L}$  corundum crucible. The measurements were performed across the temperature range 300–900 K with a constant flow of argon equal to 100  $\text{mL min}^{-1}$  and with a heating rate of 5  $\text{K min}^{-1}$ . Temperature was measured by a Pt–Pt/Rh thermocouple with an accuracy of  $\pm 0.5$  K.

Structural analysis of  $[\text{Mn}(\text{NH}_3)_6](\text{NO}_3)_2$  was undertaken using the X-ray powder diffraction (XRPD) method. The XRPD data were collected with a PANalytical X'Pert PRO powder diffractometer (operating in Bragg–Brentano geometry). The measurements continued for 2 h only because of the rapid decomposition of the title compound. In order to delay the process of decomposition, the sample was prepared as a mixture with paraffin oil. The diffraction pattern was made at an angle of  $2\theta$  with a range of 10°–80°. The lattice parameter was defined using Rietveld refinement.

The Fourier transform far infrared (FT-FIR) spectrum of  $[\text{Mn}(\text{NH}_3)_6](\text{NO}_3)_2$  (at room temperature) was recorded in the wavenumber region 600–50  $\text{cm}^{-1}$ , at a resolution of 1  $\text{cm}^{-1}$ , on a Nicolet Magna-IR 760 spectrometer equipped with a deuterium triglycine sulphate (DTGS) detector and a Globar lamp as a light source, for a powdered sample mixed with polyethylene. The Fourier transform middle-infrared (FT-MIR) spectrum at room temperature was performed with a Bruker EQUINOX 55 spectrometer, in the wavenumber range 4000–400  $\text{cm}^{-1}$ , with a resolution of 2  $\text{cm}^{-1}$ , for a sample suspended in paraffin oil (Nujol). The FT-MIR measurements of the spectra in the temperature range of 15–290 K and at the wavenumber range 4000–500  $\text{cm}^{-1}$  were carried out with the same spectrometer for a powdered sample mixed with Nujol and drifted on a KBr pellet. The temperature of the “cold finger” was measured with an accuracy of  $\pm 1$  K, but the temperature of the sample may have been several Kelvin higher.

UV–Vis reflectance spectra were measured for a sample of the title compound in  $\text{BaSO}_4$  pellet (with  $\text{BaSO}_4$  as a reference) using a Shimadzu 2101 PC spectrometer equipped with an ISR-260 attachment.

Differential scanning calorimetry (DSC) measurements were performed at 93–297 K with a PerkinElmer PYRIS 1 DSC apparatus. The instrument was calibrated using the literature data for indium and water melting points. The enthalpy change ( $\Delta H$ ) was calculated by the numerical integration of the DSC curve under the anomaly peak after a linear background arbitrary subtraction. The entropy

change ( $\Delta S$ ) was calculated using the formula  $\Delta S = \Delta H / T_c$ . The powdered sample was placed in an aluminium vessel and closed by compression. The measurements were made both on heating and on cooling a freshly synthesized sample of mass 7.90 mg with constant rates of 10, 20, 30 and 40 K min<sup>-1</sup>. Other experimental details were the same as those published in [23].

Supplementary DSC measurements were performed over the range of 250–730 K with a heating rate of 5 K min<sup>-1</sup> with a Mettler Toledo DSC 821e apparatus for a sample of mass 3.8300 mg hermetically sealed in a 40 mL aluminium crucible, with a constant flux of argon (80 mL min<sup>-1</sup>).

## Results and discussion

Spectroscopic (FT-FIR, FT-MIR, UV-Vis), structural (XRPD) and thermal (TG, DTG, QMS, SDTA) analysis of the title compound.

Figure 1 shows the far- and middle-infrared (FT-FIR and FT-MIR) spectra together with the Raman scattering

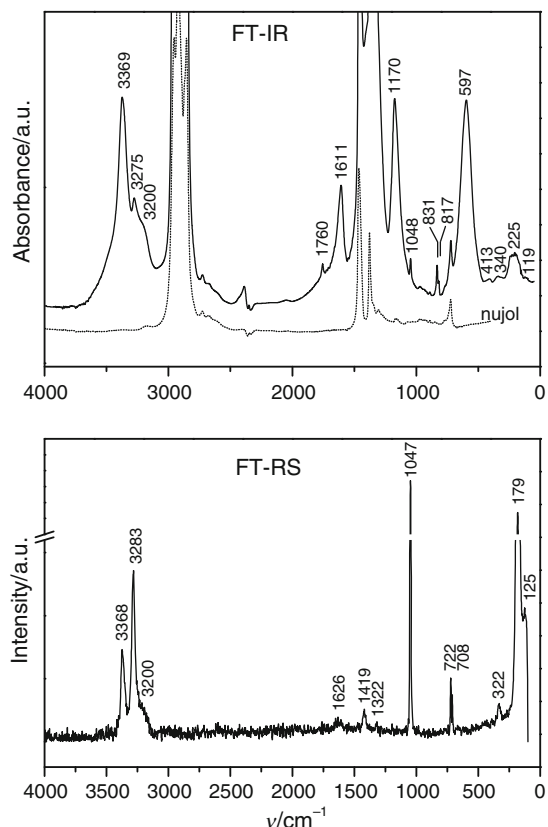


**Fig. 1** The infrared (FT-FIR and FT-MIR) and Raman scattering (FT-RS) spectra of  $[\text{Mn}(\text{NH}_3)_6](\text{NO}_3)_2$ . The FT-MIR spectrum of pure Nujol was additionally presented because the spectrum of the title compound was made in Nujol suspension

(FT-RS) spectrum for  $[\text{Mn}(\text{NH}_3)_6](\text{NO}_3)_2$ , both obtained at room temperature, for a comparison. A factor group analysis for the  $Fm\bar{3}m$  ( $O_h^5$ , No. 225) space group ( $Z = 4$ ) revealed the following 12 lattice vibrations:  $F_{1g} + 2F_{1u} + F_{2g}$ . Modes of type “u” are infrared-active only and modes of type “g” are Raman-active only. However, the rotational mode  $F_{1g}$  is spectrally inactive [24]. The  $[\text{Mn}(\text{NH}_3)_6]^{2+}$  cation was assumed to have octahedral symmetry with six nearly freely rotating ammine ligands. There are 69 normal vibrations modes for an octahedral cation of  $O_h$  symmetry:  $3A_{1g} + A_{1u} + 3E_g + E_u + 4F_{1g} + 7F_{1u} + 4F_{2g} + 4F_{2u}$ . There are 15 internal vibrations of octahedral coordination sphere ( $A_{1g} + E_g + 2F_{1u} + F_{2g} + F_{2u}$ ). 36 vibrations are the internal  $\text{NH}_3$  vibrations ( $2A_{1g} + 2E_g + 4F_{1u} + 2F_{1g} + 2F_{2g} + 2F_{2u}$ ). 18 librational vibrations may be divided into six ligand torsions ( $A_{1u} + E_u + F_{1g}$ ) and 12 ligand rocking ( $F_{1g} + F_{1u} + F_{2g} + F_{2u}$ ) modes. However, modes:  $A_{1u}$ ,  $E_u$ ,  $4F_{1g}$  and  $4F_{2u}$  are inactive both in Raman and infrared spectroscopy (27 vibrations). Thus, only 42 vibrations (12 of octahedron, 24 internal and 6 libration of  $\text{NH}_3$  (only rocking)) are active in IR and RS spectra [24]. An  $\text{NO}_3^-$  anion with a flat pyramidal shape ( $D_{3h}$  point group) has six normal vibrations of symmetry:  $A'_1$ ,  $A''_2$  and  $2E'$ . The first mode ( $v_1(\text{NO}_3^-) = v_s(\text{NO})A'_1$ ) is infrared-inactive and the second ( $v_2(\text{NO}_3^-) = v_{as}(\text{NO}_3)A''_2$ ) is Raman-inactive. The two modes of  $E'$ , namely:  $v_3(\text{NO}_3^-) = v_d(\text{NO})E'$  and  $v_4(\text{NO}_3^-) = \delta_d(\text{ONO})E'$ , are active both in the Raman and in the infrared spectrum [25]. Table 1 presents a list of the band positions observed in the FT-IR and FT-RS spectra of  $[\text{Mn}(\text{NH}_3)_6](\text{NO}_3)_2$ , as well as their relative intensities and assignments. The assignments were determined by taking into account the results of corresponding theoretical spectra of  $[\text{Mn}(\text{NH}_3)_6](\text{NO}_3)_2$  calculations, which were obtained using B3LYP/LANL2TZ+/6-311+G(d,p) level of density functionals theory (DFT) [26]. For comparison, Table 1 also includes the spectral data obtained by us for  $[\text{Cd}(\text{NH}_3)_6](\text{NO}_3)_2$  and  $[\text{Ni}(\text{NH}_3)_6](\text{NO}_3)_2$ . A combination of the assignments and a comparison with these similar compounds proved that the composition and structure of the investigated compound was correct.

In order to further verify of the composition of the title compound, the UV-Vis reflectance spectrum of solid  $[\text{Mn}(\text{NH}_3)_6](\text{NO}_3)_2$  was recorded and is presented, after Kubelka-Munk transformation [27], in Fig. 2. It was not possible to measure the spectra in aqueous solution because, after dissolution in water, it almost immediately decomposes and a dark brown product is precipitated. However, the compound in its solid state is relatively stable under atmospheric pressure of dry ammonia. Several repetitions of spectrum registration show that the complex does not undergo spectral changes over the course of several minutes. Concerning the  $[\text{Mn}(\text{NH}_3)_6](\text{NO}_3)_2$ , which has almost white colour with a very light brown tint, it

**Table 1** Frequencies of vibrations (in  $\text{cm}^{-1}$ ) obtained by IR and RS for  $[\text{M}(\text{NH}_3)_6](\text{NO}_3)_2$  compounds at room temperature, where M = Mn, Cd and Ni, and its assignments

Infrared absorption			Raman scattering			Assignments
Mn	Cd	Ni	Mn	Cd	Ni	
3369 s	3378 m, br	3346 s	3368 s	3377 m	3390 m	$\nu_{as}(\text{NH})\text{F}_{2g}$
						$\nu_{as}(\text{NH})\text{F}_{1u}$
3275 m	3262 m, sh	3242 sh	3283 vs	3285 s	3295 s	$\nu_s(\text{NH})\text{A}_{1g}$
						$\nu_s(\text{NH})\text{F}_{1u}$
3200 w, br	3208 m, sh		3200 w, br	3188 w	3195 w	$\nu_s(\text{NH})\text{E}_g$
1760 vw	1755 w	1764 w				$2\delta_{as}(\text{HNH})\text{F}_{1u}$
			1626 vw	1633 sh	1630 m	$2\nu_2(\text{NO}_3^-)\text{A}_2''$
1611 m	1606 s	1616 m				$\delta_{as}(\text{HNH})\text{F}_{2g}$
	1456 vs		1419 m	1408 m	1423 m	$\delta_{as}(\text{HNH})\text{F}_{1u}$
	1381 vs	1383 vs			1395 sh	$\nu_3(\text{NO}_3^-)\text{E}'$
	1303 s					
			1322 w	1325 w	1322 m	$\delta_s(\text{HNH})\text{A}_{1g}$
					1267 w	$\delta_s(\text{HNH})\text{E}_g$
1170 s	1156 s, br	1192 s				$\delta_s(\text{HNH})\text{F}_{1u}$
	1109 s, br					
1048 w	1046 s	1045 vw	1047 vs	1049 vs	1050 vs	$\nu_1(\text{NO}_3^-)\text{A}_1'$
831 w	832 m	826 m				$\nu_2(\text{NO}_3^-)\text{A}_2''$
817 m	819 m					
	721 m		722 s	721 m	730 s	$\nu_4(\text{NO}_3^-)\text{E}'$
	712 m		708 m	711 m	711 s	
597 s	607 s	677 m				$\rho(\text{NH}_3)\text{F}_{1u}$
			440 vw?	?	?	$\rho(\text{NH}_3)\text{F}_{2g}$
413 vw	563 s					
	334 w	374 vw				
340 w						$\nu_{as}(\text{MnN})\text{F}_{1u}$
		327 w				$\nu_{as}(\text{NiN})\text{F}_{1u}$
	286 m					$\nu_{as}(\text{CdN})\text{F}_{1u}$
					376 s	$\nu_s(\text{NiN})\text{A}_{1g}$
225 m				351 m		$\nu_s(\text{CdN})\text{A}_{1g}$
			322 m			$\nu_s(\text{MnN})\text{A}_{1g}$
						$\delta_{as}(\text{NMnN})\text{F}_{1u}$
		223 m				$\delta_{as}(\text{NNiN})\text{F}_{1u}$
	165 m					$\delta_{as}(\text{NCdN})\text{F}_{1u}$
					240 sh	$\nu_{as}(\text{NiN})\text{E}_g$
				185 m		$\nu_{as}(\text{CdN})\text{E}_g$
			179 vs			$\nu_{as}(\text{MnN})\text{E}_g$
					240 s	$\delta_{as}(\text{NNiN})\text{F}_{2g}$
				150 s		$\delta_{as}(\text{NCdN})\text{F}_{2g}$
			125 s			$\delta_{as}(\text{NMnN})\text{F}_{2g}$
119 vw	100 w					$\nu_{L(lattice)}\text{F}_{1u}$
					108 m	$\nu_{L(lattice)}\text{F}_{2g}$
						$\nu_{L(lattice)}\text{F}_{2g}$

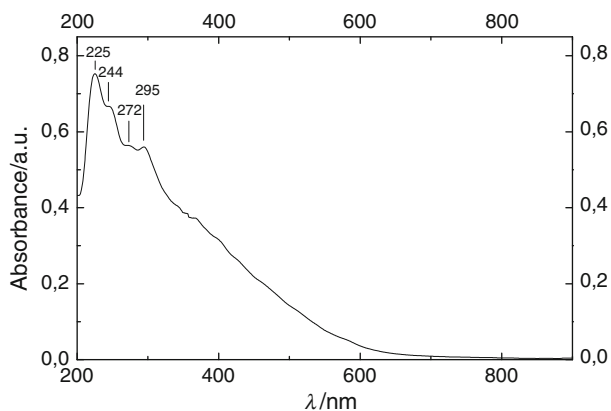


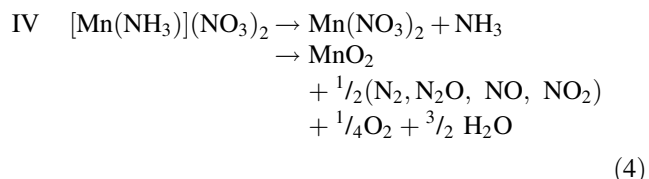
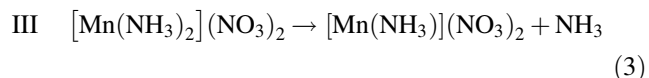
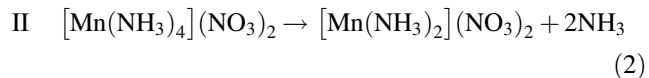
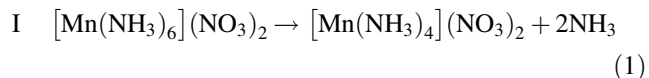
**Fig. 2** UV-Vis spectrum of polycrystalline  $[\text{Mn}(\text{NH}_3)_6](\text{NO}_3)_2$  mixed with  $\text{BaSO}_4$

seems that  $d-d$  transitions are not possible. The position of  $\text{NH}_3$  ligands and Mn(II) in the spectrochemical series ( $f = 1.25$ ,  $g = 8.0$ ) together with the observed reflectance spectrum suggest that Mn(II) with a  $d^5$  configuration forms a high-spin complex. Therefore,  $d-d$  transition is spin forbidden and is not visible in the spectra. The observed reflectance spectrum indicates an almost constant increase in absorbance below 630 nm without a maximum. Such behaviour is typical for semiconductors and may indicate electron delocalization in the solid state. The bands at 295, 272, 244, and 225 nm, not well separated, are only observed in the UV range and can be attributed to intra-ligand transitions probably overlapped with charge-transfer bands from ligand to metal. Two last bands (at 225 with a shoulder at 244) were also observed in  $[\text{Co}(\text{NH}_3)_6](\text{NO}_3)_2$ , what can support their intra ligand origin [21]. Bands at 272 and 295 were not observed in Co(II) complex, this can be a result of either their low intensity and overlapping with  $d-d$  transition in Co(II) or lower energy of ligand-to-metal transition (due to lower  $d-d$  orbital splitting,  $g = 8.0$  for  $\text{Mn}^{2+}$  and 9.0 for  $\text{Co}^{2+}$ ).

In order to further verify the composition of the title compound, an XRPD measurement was made. The diffraction pattern of  $[\text{Mn}(\text{NH}_3)_6](\text{NO}_3)_2$  obtained at room temperature can be indexed as a regular system; space group No. 225 =  $Fm \bar{3}m = O_h^5$ ; with the lattice parameter  $a = 11.0056 \text{ \AA}$  and with four molecules in the unit cell ( $Z = 4$ ). The compound has a fluorite (C1) type structure typical for  $\text{K}_2\text{PtCl}_6$ . The structural parameters are very similar to those for other ionic hexaamminemetall(II) complexes [1–6].

Thermal analysis was the next step in the identification of the title compound. Figure 3 presents the TG, DTG, QMS and SDTA curves for the temperature range 300–800 K. Only QMS curves for  $m/z = 17, 18, 28, 30, 32, 44$  and 46, which correspond to:  $\text{NH}_3$ ,  $\text{H}_2\text{O}$ ,  $\text{N}_2$ ,  $\text{NO}$ ,  $\text{O}_2$ ,  $\text{N}_2\text{O}$

and  $\text{NO}_2$ , respectively, are shown. These results show that the thermal decomposition of the investigated compound takes place in four main stages (I–IV):



In the first (I) stage,  $\frac{2}{6}$  of all  $\text{NH}_3$  ligands were seceded. Stages II and III are connected with an abruptness of the next  $\frac{2}{6}$  and  $\frac{1}{6}$  of all  $\text{NH}_3$ , respectively, and  $[\text{Mn}(\text{NH}_3)](\text{NO}_3)_2$  was finally formed. The last  $\text{NH}_3$  molecule per formula unit was abruptly at stage IV and immediate simultaneous decomposition of the nitrate(V) took place. Thus, nitrogen oxides, oxygen and water were freed and solid  $\text{MnO}_2$  was finally formed. At 750 K, an additional small loss of mass of the sample was observed, which can be associated with the decomposition of  $\text{MnO}_2$  to  $\text{Mn}_2\text{O}_3$ :



This statement confirms the presence of the second peak on the QMS curve for  $m/z = 32$  because additional oxygen is given off during this decomposition (see Eq. 5 and Fig. 3).

Of course, it is possible that somewhat different products are formed in stage IV due to temporary concentrations of particular substrates. It is, therefore, very difficult to give precise equations for these reactions. Nevertheless, both Małecka [28] and Shoheen and Hong [29] also had observed similar products of thermal decompositions of  $[\text{Mn}(\text{H}_2\text{O})_6](\text{NO}_3)_2$  and  $[\text{Mn}(\text{H}_2\text{O})_4](\text{NO}_3)_2$ , respectively. Table 2 shows temperature ranges, experimental and calculated percentage mass losses, masses after decomposition and the proposed products formed during particular stages of the thermal decomposition of  $[\text{Mn}(\text{NH}_3)_6](\text{NO}_3)_2$ .

The progress of thermal decomposition of  $[\text{Mn}(\text{NH}_3)_6](\text{NO}_3)_2$  described above is consistent with the results of supplementary DSC measurements performed in the range of 250–730 K. Figure 4 shows the DSC curve with three endo- and one exothermic peaks. The three endothermic peaks are connected with the three-stage process of the deammination and, the fourth exothermic with more complex processes which consist mainly of manganese(II)

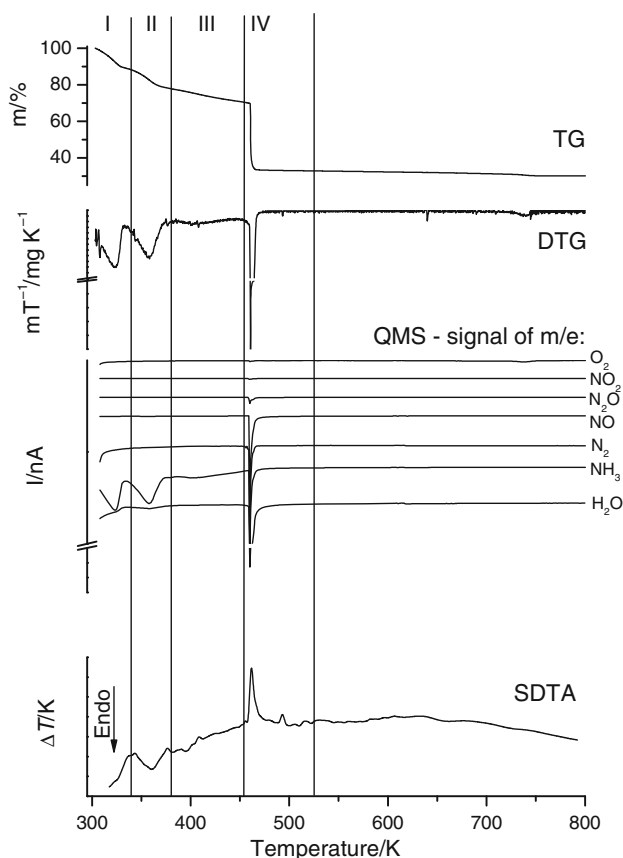


**Fig. 3** TG, DTG, QMS and SDTA curves registered for  $[\text{Mn}(\text{NH}_3)_6](\text{NO}_3)_2$  at 300–873 K with constant heating rate of  $5 \text{ K min}^{-1}$  (corundum vessel)

nitrate(V) decomposition and simultaneous ammonia oxidation (see Eq. 4).

#### Phase transitions investigations (DSC)

Differential scanning calorimetry measurements for  $[\text{Mn}(\text{NH}_3)_6](\text{NO}_3)_2$  were performed in the temperature range 90–297 K with scanning rates of 10, 20 and  $30 \text{ K min}^{-1}$  for two different samples of masses: 8.23 mg

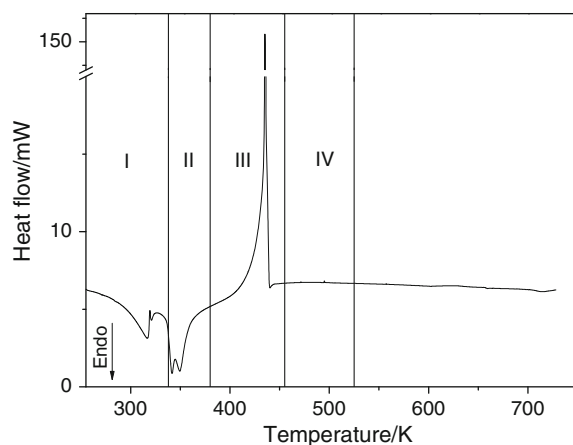


**Fig. 4** DSC curve for  $[\text{Mn}(\text{NH}_3)_6](\text{NO}_3)_2$  registered at 280–720 K with constant heating rate  $5 \text{ K min}^{-1}$  (I–IV denotes stages of the thermal decomposition)

(sample a) and 5.50 mg (sample b). Figure 5 shows the temperature dependences of the heat flows (DSC curves) obtained for the title compound on heating (upper curve) and on cooling (lower curve) exemplarily for the sample b, at the rate of  $30 \text{ K min}^{-1}$ . Two distinct anomalies on the DSC curves were registered at all scanning rates: a large one ( $\overline{\Delta S_1} = 20.8 \text{ J mol}^{-1} \text{ K}^{-1}$ ) at:  $T_{C1}^h = 207.8 \text{ K}$  and  $T_{C1}^c = 207.2$ , and the a second smaller one ( $\overline{\Delta S_2} = 8.6 \text{ J mol}^{-1} \text{ K}^{-1}$ ) at:  $T_{C2}^h = 184.4 \text{ K}$  and  $T_{C2}^c = 160.8 \text{ K}$  (where indexes h and c denote heating and cooling of the sample, respectively).  $\overline{\Delta S_n}$  denotes mean values of entropy changes calculated for the detected anomalies at heating and cooling of the sample. The phase transition temperatures were calculated by extrapolating the dependence of the corresponding  $T_{\text{peak}}^h$  and  $T_{\text{peak}}^c$  values against the scanning rate of heating and cooling the samples to the scanning rate value of  $0 \text{ K min}^{-1}$ . These values correspond well to the onset of peaks in corresponding DSC curves. The presence of thermal hysteresis of the phase transitions and the sharpness of the heat flow anomalies attests that the detected phase transitions are of the first-order type. Large value of thermal hysteresis ( $\sim 24 \text{ K}$ ) of the phase transition

**Table 2** Temperature range, percentage mass loss and the products of thermal decomposition of  $[\text{Mn}(\text{NH}_3)_6](\text{NO}_3)_2$  (heating rate  $5 \text{ K min}^{-1}$ , in corundum vessel)

Mass of the sample/K	Stage number	Temperature range/K	Mass loss/%	Mass after decomposition/%	Calculated values/%	Products of thermal decomposition
8.9733	I	305–337	11.34	–	12.12	$2\text{NH}_3$
	II	338–380	10.87	–	12.12	$2\text{NH}_3$
	III	381–455	7.29	–	6.06	$1\text{NH}_3$
	IV	456–525	37.60	–	38.79	$1\text{NH}_3 + (\text{NO}, \text{N}_2\text{O}, \text{N}_2, \text{O}_2, \text{NO}_2, \text{H}_2\text{O})$
				32.9	30.91	$\text{MnO}_2$

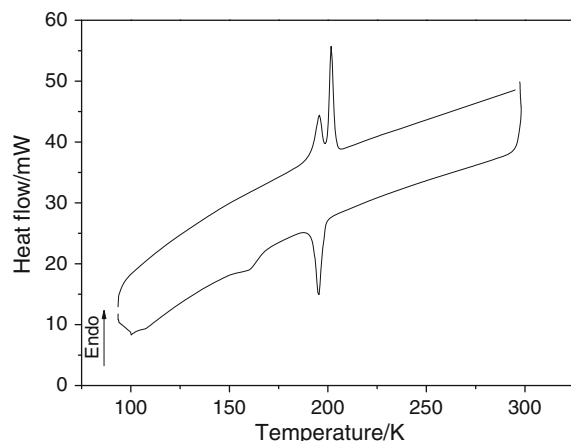


**Fig. 5** DSC curves for  $[\text{Mn}(\text{NH}_3)_6](\text{NO}_3)_2$  registered at 95–293 K with a scanning rate of  $30 \text{ K min}^{-1}$  at cooling (lower curve) and at heating (upper curve)

at  $T_{C2}$  is very characteristic for similar compounds with high degree of dynamical disorder of  $\text{NO}_3^-$  anions [7, 11]. The mean values of the enthalpy and entropy changes of the detected phase transitions are shown in Table 3. The values of the entropy changes accompanying the phase transitions suggest their “order–disorder” mechanism.

Molecular motions versus phase transition (IR bands shape vs.  $T$ )

The FT-MIR spectra of  $[\text{Mn}(\text{NH}_3)_6](\text{NO}_3)_2$ , within the wavenumber range  $4000$ – $400 \text{ cm}^{-1}$ , were registered during the cooling of the sample from 295 to 15 K. In most  $[\text{M}(\text{NH}_3)_6]\text{X}_2$  compounds with dynamical orientation disorder of ammonia molecules [29], fast  $\text{NH}_3$  reorientation does not stop at phase transitions. Therefore, among other things, we would like to check whether the observed phase transitions in the title compound are or are not connected with a drastic change in the reorientation dynamics of the  $\text{NH}_3$  ligands. We would also like to compare the obtained results with those obtained by us earlier for  $[\text{Ni}(\text{NH}_3)_6](\text{NO}_3)_2$  and  $[\text{Mg}(\text{NH}_3)_6](\text{NO}_3)_2$  [14]. A study of the full with at half maximum (FWHM) of the infrared bands connected with mode  $\delta_s(\text{HNH})\text{F}_{1u}$  (at ca.  $1170 \text{ cm}^{-1}$ ) in the function of temperature was made. It would be also

very interesting to check whether the observed phase transitions are or are not connected with a drastic change in the reorientational dynamics of the  $\text{NO}_3^-$  anions. However, we did not perform similar study of the infrared active modes of nitrate(V) anion:  $v_3(\text{NO}_3^-)\text{E}' = 1375 \text{ cm}^{-1}$  and  $v_4(\text{NO}_3^-)\text{E}' = 721 \text{ cm}^{-1}$ , because they are masked by the Nujol bands. Unfortunately, the sample of  $[\text{Mn}(\text{NH}_3)_6](\text{NO}_3)_2$  interact with other than Nujol media (KBr, Hexachlorobutadiene, Fluorolab) and decomposes very easily by itself.

We followed the analysis of FWHM versus temperature, described by Carabatos-Nédelec and Becker [30, 31]. We assumed that the reorientation correlation time  $\tau_R$  is the mean time between instantaneous jumps from one potential well to another and is defined as

$$\tau_R = \tau_0 \exp\left(\frac{E_a}{RT}\right), \quad (6)$$

where  $\tau_0$  is the relaxation time at infinite temperature  $T$ ,  $E_a$  is the height of the potential barrier for reorienting species and  $R$  is the gas constant. For vibrations of frequency  $\omega > 1 \times 10^{13} \text{ s}^{-1}$  and for  $\tau_R > 1 \times 10^{-12} \text{ s}$ , the temperature dependence of the FWHM can be described by [30–33]:

$$\text{FWHM}(T) = (a + bT) + c \exp\left(-\frac{E_a}{RT}\right), \quad (7)$$

where  $a$ ,  $b$ ,  $c$  and  $E_a$  are parameters to fit. The linear part of Eq. 7 corresponds to the bandwidth associated with vibrational relaxation and the exponential term corresponds to the bandwidth associated with reorientational relaxation.

The FWHM values of selected infrared bands were calculated by fitting to them the Lorentz function using the ORIGIN program. Figure 6 shows the temperature dependences of the FWHM of the band associated with the  $\delta_s(\text{HNH})\text{F}_{1u}$  mode located at ca.  $1170 \text{ cm}^{-1}$ . We carried out the fitting of Eq. 7 to FWHM vs.  $T$  dependence in two different ways. The first fitting was done to all experimental points in the temperature range 295–15 K. The fitted parameters are listed in Table 4. The estimated value for the activation energy of the reorientational motion of the  $\text{NH}_3$  ligands is  $E_a = 11.9 \text{ kJ mol}^{-1}$ . The second fitting

**Table 3** Thermodynamic parameters of the phase transitions of  $[\text{Mn}(\text{NH}_3)_6](\text{NO}_3)_2$

Parameters	Large anomaly		Small anomaly	
	Cooling	Heating	Cooling	Heating
$T_C/\text{K}$	$207.16 \pm 0.10$	$207.81 \pm 0.10$	$160.78 \pm 0.10$	$184.36 \pm 0.10$
$\Delta\bar{H}/\text{kJ mol}^{-1}$	$4.40 \pm 0.64$	$3.95 \pm 0.35$	$1.03 \pm 0.46$	$2.09 \pm 0.26$
$\Delta\bar{S}/\text{J mol}^{-1} \text{ K}^{-1}$	$22.10 \pm 3.64$	$19.41 \pm 1.77$	$6.40 \pm 2.86$	$10.89 \pm 1.29$

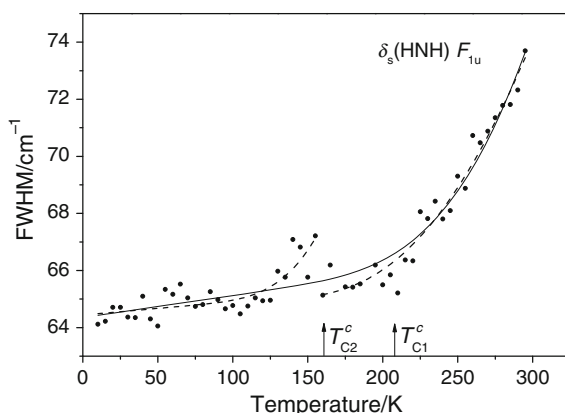


**Fig. 6** Temperature dependence of FWHM of  $\delta_s(\text{HNH})\text{F}_{1u}$  infrared band at  $1170 \text{ cm}^{-1}$ . Arrows denote phase transitions temperatures registered by DSC at cooling of the  $[\text{Mn}(\text{NH}_3)_6](\text{NO}_3)_2$  sample. Solid line represents fitting of Eq. 7 to the whole experimental points (from temperature range 295–15 K). Broken line represents fitting of Eq. 7 to the experimental points from temperature ranges 295–160 and 161–15 K, respectively

was done separately for points registered before and after the phase transition temperature  $T_{C2}^c = 160.8 \text{ K}$ , that is for the points from temperature ranges 295–160 K and 161–15 K, respectively. The fitted parameters are listed in Table 4. In this way, the estimated values of the activation energies for the reorientational motions of the  $\text{NH}_3$  ligands are:  $E_a(\text{I,II}) = 9.9 \text{ kJ mol}^{-1}$  for the high and intermediate phases and  $E_a(\text{III}) = 7.7 \text{ kJ mol}^{-1}$  for the low temperature phase. These values are only a little higher than those for  $[\text{Ni}(\text{NH}_3)_6](\text{NO}_3)_2$  ( $4.7$  and  $2.3 \text{ kJ mol}^{-1}$ ) or for  $[\text{Mg}(\text{NH}_3)_6](\text{NO}_3)_2$  ( $7.1$  and  $2.6 \text{ kJ mol}^{-1}$ ), respectively, as derived from quasielastic neutron scattering (QENS) measurements [10–16].

The results obtained suggest that the reorientational motions of the  $\text{NH}_3$  ligands do not contribute to the mechanism of phase transition at  $T_{C1}^c$  but, in the phase transition at  $T_{C2}^c$ , the reorientational dynamic of  $\text{NH}_3$  is distinctly perturbed, very probably because of a slowing down of  $\text{NO}_3^-$  anions reorientation and a change in the symmetry of the crystal lattice as was proved to be the case for  $[\text{Ni}(\text{NH}_3)_6](\text{NO}_3)_2$  and  $[\text{Mg}(\text{NH}_3)_6](\text{NO}_3)_2$  [19].

**Table 4** Fitting parameters:  $a$ ,  $b$ ,  $c$  and  $E_a$  of the temperature dependence of FWHM of the band associated with  $\delta_s(\text{HNH})\text{F}_{1u}$  ( $\sim 1170 \text{ cm}^{-1}$ ) mode obtained for different phases of  $[\text{Mn}(\text{NH}_3)_6](\text{NO}_3)_2$

$[\text{Mn}(\text{NH}_3)_6](\text{NO}_3)_2$	Analyzed mode (band): $\delta_s(\text{HNH})\text{F}_{1u}$ ( $\sim 1170 \text{ cm}^{-1}$ )	Phases I, II and III	Phases I and II	Phase III
Fitting parameters		Phases I, II and III	Phases I and II	Phase III
$a/\text{cm}^{-1}$	65.0	65.5	64.6	
$b/\text{cm}^{-1} \text{ K}^{-1}$	$2.3 \times 10^{-3}$	$-4.0 \times 10^{-3}$	$2.0 \times 10^{-3}$	
$c/\text{cm}^{-1}$	1046.4	525.6	865.6	
$E_a/\text{kJ mol}^{-1}$	11.9	9.9	7.7	

## Conclusions

- [ $\text{Mn}(\text{NH}_3)_6](\text{NO}_3)_2$  at room temperature has a regular (cubic) structure (space group No. 225 =  $Fm\bar{3}m = O_5^h$ ) with the lattice parameter  $a = 11.0441 \text{ \AA}$  and with four molecules in the unit cell ( $Z = 4$ ).
- The DSC measurements of  $[\text{Mn}(\text{NH}_3)_6](\text{NO}_3)_2$  performed in the temperature range 90–297 K showed two anomalies in the heat flow associated with first-order type phase transitions: a large one ( $\Delta S_1 = 20.8 \text{ J mol}^{-1} \text{ K}^{-1}$ ) and a small one ( $\Delta S_2 = 8.6 \text{ J mol}^{-1} \text{ K}^{-1}$ ), both connected with the of the). The entropy change values accompanying these phase transitions suggest an “order–disorder” mechanism. The temperatures of these phase transitions, obtained by extrapolating the values obtained at different scanning rates to the zero scanning rate, were:  $T_{C1}^h = 207.8 \text{ K}$  and  $T_{C1}^c = 207.2 \text{ K}$  and  $T_{C2}^h = 184.4 \text{ K}$  and  $T_{C2}^c = 160.8 \text{ K}$  (where indexes h and c denote heating and cooling of the sample, respectively). The large thermal hysteresis (ca. 24 K) of the phase transition detected at  $T_{C2}$  is very characteristic of the hexaamminemetal(II) nitrates(V).
- The temperature dependence of the FWHM of the band associated with the  $\delta_s(\text{HNH})\text{F}_{1u}$  mode indicates fast reorientation of the  $\text{NH}_3$  ligands with reorientational correlation times in the order of picoseconds and with mean values of the activation energies:  $E_a(\text{I,II}) = 9.9 \text{ kJ mol}^{-1}$  for phases I and II and  $E_a(\text{III}) = 7.7 \text{ kJ mol}^{-1}$  for phase III. Thus, fast reorientation, at least of some part  $\text{NH}_3$  ligands “outlast” both phase transitions.
- Thermal decomposition of the investigated compound takes place in four main stages (I–IV). In the first stage (I),  $2/6$  of all  $\text{NH}_3$  ligands were seceded. Stages II and III are connected with the abruption of the next  $2/6$  and  $1/6$  of all  $\text{NH}_3$ , respectively, and  $[\text{Mn}(\text{NH}_3)](\text{NO}_3)_2$  was formed. The last molecule of  $\text{NH}_3$  per formula unit was evolved together with the simultaneous decomposition of the resulting  $\text{Mn}(\text{NO}_3)_2$  leading to the formation of gaseous products of the decomposition ( $\text{O}_2$ ,  $\text{H}_2\text{O}$ ,  $\text{N}_2$ , nitrogen oxides) and solid  $\text{MnO}_2$ .

**Acknowledgements** We are very grateful to Professor St. Wróbel, Ph.D., Dr. habil., from the Faculty of Physics, Astronomy and Applied Computer Science of the Jagiellonian University for enabling us to perform DSC measurements. Our thanks are also due to J. Chruściel, Ph.D., Dr. habil., from Faculty of Science of the University of Podlasie in Siedlce for registering the FT-FIR spectrum of our sample.

## References

1. Wyckoff RWG. The composition and crystal structure of nickel nitrate hexammoniate. *J Am Chem Soc.* 1922;44:1260–6.
2. Wyckoff RWG. Crystal structures, vol. 3. New York: Interscience; 1965.
3. Jü SH. Evidence of abnormal behaviour of  $\text{NO}_3^-$  in the cubic crystal  $\text{Ni}(\text{NO}_3)_3 \cdot 6\text{NH}_3$ . *Nature.* 1938;141:158–9.
4. Jü SH. Formation of a double crystal aggregate and the structure of the intermediate temperature modification of  $\text{Ni}(\text{NO}_3)_3 \cdot 6\text{NH}_3$ . *Nature.* 1942;150:347–9.
5. Hodorowicz S, Czerwonka J, Janik JM, Janik JA. X-ray powder diffraction studies of the thermal transformations in solid  $[\text{Ni}(\text{NH}_3)_6](\text{NO}_3)_2$ . *Physica B.* 1981;111:155–9.
6. Andresen AF, Fjellvåg H, Janik JA, Mayer J, Ściesiński J, Janik JM, et al. Adiabatic calorimetry and neutron diffraction studies of phases and phase transitions in  $[\text{Ni}(\text{ND}_3)_6](\text{NO}_3)_2$ . *Physica B.* 1986;138:295–304.
7. Migdał-Mikuli A, Mikuli E, Rachwalska M, Stanek T, Janik JM, Janik JA. An adiabatic calorimetry study of  $[\text{Ni}(\text{NH}_3)_6](\text{NO}_3)_2$ . *Physica B.* 1981;104:331–6.
8. Jenkins TE, Ferris LTH, Bates AR, Gillard RD. A Raman study of the orientational phase transitions of hexammine nickel (II) nitrate. *J Phys C.* 1978;11:L77–81.
9. Trybuła Z, Stankowski J. Phase transitions in  $[\text{Ni}(\text{NH}_3)_6](\text{NO}_3)_2$ . *Physica B.* 1988;154:87–92.
10. Belushkin AV, Janik JA, Janik JM, Natkaniec I, Otnes K. Low temperature measurements of incoherent inelastic and quasi-elastic neutron scattering in  $[\text{Ni}(\text{NH}_3)_6](\text{NO}_3)_2$ , with a simultaneous control of phase. *Physica B.* 1985;128:289–91.
11. Janik JA, Janik JM, Migdał-Mikuli A, Mikuli E, Rachwalska M, Stanek T, et al. Calorimetry, proton magnetic resonance and quasielastic neutron scattering studies of  $[\text{Mg}(\text{NH}_3)_6](\text{NO}_3)_2$ . *Physica B.* 1983;122:315–20.
12. Janik JA, Janik JM, Migdał-Mikuli A, Mikuli E, Stanek T. Comparison of calorimetry and neutron scattering results concerning phase transitions in  $[\text{Ni}(\text{NH}_3)_6](\text{NO}_3)_2$  with the Raman band profile study. *J Mol Struct.* 1984;115:5–10.
13. Janik JM, Janik JA, Pick RM, le Postollec M. Raman study of molecular motions in relation to phase transitions in  $[\text{Ni}(\text{NH}_3)_6](\text{NO}_3)_2$ . *J Raman Spectrosc.* 1987;18:493–5.
14. Migdał-Mikuli A, Mikuli E. Connection between reorientational motions of the  $\text{NH}_3$  groups and the phase transitions in  $[\text{Ni}(\text{NH}_3)_6](\text{NO}_3)_2$  and  $[\text{Mg}(\text{NH}_3)_6](\text{NO}_3)_2$  compounds. *Acta Physiol Pol A.* 1995;88:259–64.
15. Kearley GJ, Blank H.  $\text{NH}_3$  reorientation in phases I, II, and III of  $[\text{Ni}(\text{NH}_3)_6](\text{NO}_3)_2$ . *Can J Chem.* 1988;66:692–7.
16. Janik JA, Janik JM, Migdał-Mikuli A, Mikuli E, Otnes K. Incoherent quasielastic neutron scattering study of  $\text{NH}_3$  reorientations in various phases of  $[\text{Ni}(\text{NH}_3)_6](\text{NO}_3)_2$ . *Physica B.* 1981;111:62–7.
17. Belushkin A, Janik JA, Janik JM, Janik B, Migdał-Mikuli A, Mikuli E, et al. Incoherent inelastic and quasielastic neutron scattering with simultaneous neutron diffraction control of phase transitions in  $[\text{Mg}(\text{NH}_3)_6](\text{NO}_3)_2$ . *Physica B.* 1985;128:292–6.
18. Piekara-Sady L, Krupski M, Stankowski J, Gajda D. Evidence of hydrogen bonds in  $[\text{Ni}(\text{NH}_3)_6](\text{NO}_3)_2$ . *Physica B.* 1986;138:118–24.
19. Janik JM, Janik JA, Migdał-Mikuli A, Mikuli E, Otnes K. Neutron quasielastic scattering results for  $[\text{Me}(\text{NH}_3)_6](\text{XY}_4)_2$ ,  $[\text{Me}(\text{NH}_3)_6](\text{XY}_3)_2$  and  $[\text{Me}(\text{NH}_3)_6]\text{X}_2$  compounds, compared with the calorimetric and Raman line width data—a new analysis. *Physica B.* 1991;168:45–52.
20. Migdał-Mikuli A, Liszka-Skoczyłas M, Mikuli E. Phase transition and molecular motions in  $[\text{Cd}(\text{NH}_3)_6](\text{NO}_3)_2$ . *Phase Transit.* 2007;80:547–57.
21. Liszka-Skoczyłas M, Mikuli E, Szklarzewicz J, Hetmańczyk J. Thermal behaviour, phase transition and molecular motions in  $[\text{Co}(\text{NH}_3)_6](\text{NO}_3)_2$ . *Thermochim Acta.* 2009;496:38–44.
22. Mikuli E, Liszka M, Molenda M. Thermal decomposition of  $[\text{Cd}(\text{NH}_3)_6](\text{NO}_3)_2$ . *J Therm Anal Calorim.* 2007;89:573–8.
23. Migdał-Mikuli A, Mikuli E, Wróbel S, Hetmańczyk Ł. DSC investigations of the phase transitions of  $[\text{M}(\text{NH}_3)_6](\text{ClO}_4)_2$  and  $[\text{M}(\text{NH}_3)_6](\text{BF}_4)_2$ , where  $\text{M} = \text{Co}$  and  $\text{Cd}$ . *Z Naturforsch A.* 1999;54:590–4.
24. Schmidt KH, Müler A. Vibrational spectra and force constants of pure ammine complexes. *Coord Chem Rev.* 1976;19:41–97.
25. Nakamoto K. Infrared and Raman spectra of inorganic and coordination compounds. 5th ed. NY: Wiley-Interscience Publication; 1997
26. Drużbicki K, Mikuli E. Experimental (FT-IR and FT-RS) and theoretical (DFT) studies of molecular structure and internal modes of  $[\text{Mn}(\text{NH}_3)_6](\text{NO}_3)_2$ . *Spectrochim Acta A* (to be published).
27. Kubelka P, Munk F. Ein Beitrag zur Optik der Farbanstriche. *Z Tekn Phys.* 1931;12:593–601.
28. Małecka B. Rozprawy i Monografie, vol. 144. Kraków: UWND AGH; 2005. in polish.
29. Shoheen WM, Hong KS. Thermal characterisation and physico-chemical properties of  $\text{Fe}_2\text{O}_3\text{-Mn}_2\text{O}_3/\text{Al}_2\text{O}_3$  systems. *J Therm Anal Calorim.* 2002;68:289–306.
30. Schiebel P, Prandl W. Single particle dynamics in an anharmonic potential with translation-rotation coupling: crossover from weak localisation via chaos to free rotation. *Z Phys B.* 1997;104:137–45.
31. Carabatos-Nédelec C, Becker P. Order-disorder and structural phase transitions in solid-state materials by Raman Scattering analysis. *J Raman Spectrosc.* 1997;28:663–72.
32. Andrade P da R, Prasad Rao AD, Katiyar RS, Porto SPS. Analysis of the relationship between temperature dependence of the libration mode and dielectric relaxation in  $\text{NaNO}_2$ . *Solid State Commun.* 1973;12:847–51.
33. Bator G, Jakubas R, Baran J. Vibrational study of the structural phase transitions in the  $(\text{CH}_3\text{ND}_3)_3\text{Sb}_2\text{Br}_9$  (d-MABA) crystals by infrared spectroscopy. *Vib Spectrosc.* 2001;25:101–13.